

# An Improved Shashlyk Calorimeter

G.S. Atoian<sup>a,c</sup>, G.I. Britvich<sup>b</sup>, S.K. Chernichenko<sup>b</sup>,  
 S. Dhawan<sup>c</sup>, V.V. Issakov<sup>a,c</sup>, O.V. Karavichev<sup>a</sup>,  
 T.L. Karavicheva<sup>a</sup>, V.N. Marin<sup>a</sup>, A.A. Poblaguev<sup>a,c,\*</sup>,  
 I.V. Shein<sup>b</sup>, A.P. Soldatov<sup>b</sup>, and M.E. Zeller<sup>c</sup>

<sup>a</sup>*Institute for Nuclear Research of Russian Academy of Sciences, Moscow 117312, Russia*

<sup>b</sup>*Institute for High Energy Physics, Protvino 142284, Russia*

<sup>c</sup>*Physics Department, Yale University, New Haven, CT 06511, USA*

---

## Abstract

Shashlyk electromagnetic calorimeter modules with an energy resolution of about  $3\%/\sqrt{E}$  (GeV) for 50–1000 MeV photons has been developed, and a prototype tested. Details of these improved modules, including mechanical construction, selection of wave shifting fibers and photo-detectors, and development of a new scintillator with improved optical and mechanical properties are described. How the modules will perform in a large calorimeter was determined from prototype measurements. The experimentally determined characteristics of the calorimeter prototype show energy resolution of  $\sigma_E/E = (1.96 \pm 0.1)\% \oplus (2.74 \pm 0.05)\%/\sqrt{E}$ , time resolution of  $\sigma_T = (72 \pm 4)/\sqrt{E} \oplus (14 \pm 2)/E$  (ps), where photon energy  $E$  is given in GeV units and  $\oplus$  means a quadratic summation. A punch-through inefficiency of photon detection was measured to be  $\epsilon \approx 5 \times 10^{-5}$  ( $\Theta_{\text{beam}} > 5$  mrad).

*Key words:* Shashlyk calorimeter, scintillator, WLS fiber, APD, WFD, Monte-Carlo simulation

*PACS:* 29.40.Vj, 07.05.Tp

---

## 1 Introduction.

The Shashlyk technique for electromagnetic calorimetry [1] has been in use for several years. In designing a large calorimeter for the KOPIO experiment

---

\* Corresponding author. *E-mail address:* poblaguev@bnl.gov (A.A. Poblaguev)

[2] we have developed an improved Shashlyk module for such a device. This paper describes the design and construction of the module, as well as the unit’s performance in prototype tests. It is further development of the work described in Ref [3].

The requirements of the KOPIO experiment led to the following specifications:

- Energy range: 50–1000 MeV.
- Energy resolution:  $\approx 3.0\%/\sqrt{E(\text{GeV})}$ .
- Time resolution:  $\approx 100 \text{ ps} / \sqrt{E} (\text{GeV})$ .
- Effective noise per channel:  $\leq 0.5 \text{ MeV}$
- Photon detection inefficiency:  $\leq 10^{-4}$ .
- Granularity:  $\sim 10 \text{ cm}$ .
- Size of the Calorimeter:  $4.4 \times 4.4 \text{ m}^2$ .
- Operation in a magnetic field of up to 500 Gauss.

The Shashlyk approach, in which modules are constructed of lead-scintillator sandwiches read out by means of Wavelength-Shifting (WLS) fibers passing through holes in the scintillator and lead is appropriate for such specifications. The performance level can be achieved economically with well understood and reliable techniques. We describe a module with significantly improved performance over previous manifestations for which the technique is well proved by us, *e.g.* experiment E865 at Brookhaven [1,4], and has been adopted by others, *e.g.* the PHENIX RHIC detector [5], the HERA-B detector at DESY [6], and the LHCb detector at CERN [7].

## 2 Approach to improving the Shashlyk module

At the outset of improving the module a detailed simulation model was developed [3]. This model is based on a GEANT3 [8] description of electromagnetic shower and a special optical simulation of the light collection in the scintillator plates. Input for the model was experimental and test beam data. The model output correlated well with data. Analyzing the performance of the prototype Shashlyk module with energy resolution of about  $4\%/\sqrt{E(\text{GeV})}$ <sup>1</sup> we found, that energy resolution of about  $3.0\%/\sqrt{E(\text{GeV})}$  could be reached after some optimization of the module’s mechanical and optical properties (see details in Ref. [3]).

We revisited the mechanical and optical construction as described below, and

---

<sup>1</sup> This module was described in details in Ref. [3]. In this paper we will refer to it as to “earlier” Shashlyk module.

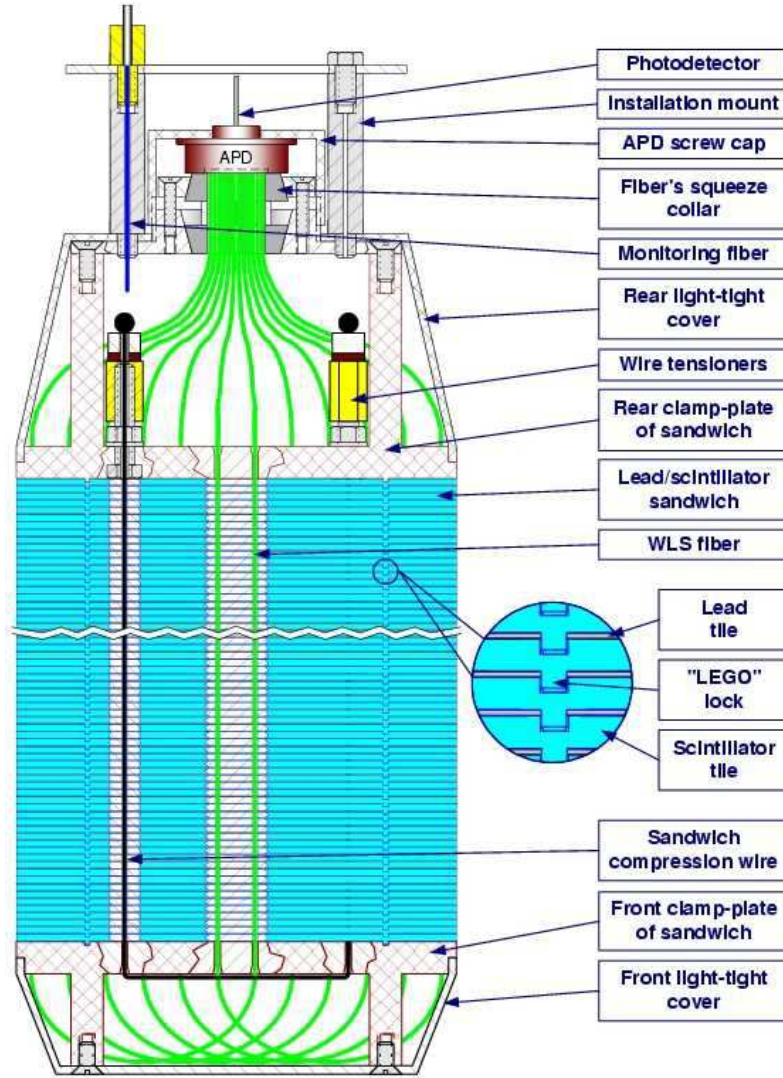


Fig. 1. The Shashlyk module design.

optimized the selection of WLS fibers and the photo-detector. A new scintillator with improved optical and mechanical properties was specially developed at the IHEP scintillator facility (Protvino, Russia) [9]. The corresponding improvements to the module design were implemented in the new KOPIO Calorimeter prototype modules, which were equipped with an Avalanche Photo Diode (APD) and Wave-Form Digitizer (WFD) readout.

### 2.1 Mechanical construction of the improved Shashlyk module.

The design of the new prototype module is shown in Figures 1, 2. The module is a sandwich of alternating perforated stamped lead and injection-molded polystyrene-based scintillator plates. The cross sectional size of a module is

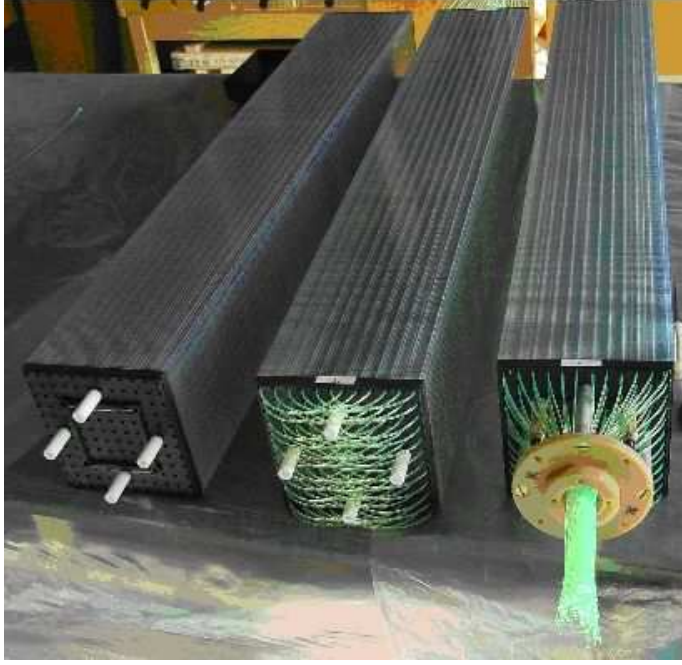


Fig. 2. The Shashlyk modules at different stages of assembly.

$110 \times 110 \text{ mm}^2$ . There are 300 layers, each layer consisting of a 0.275-mm lead plate and 1.5-mm scintillator plate. The lateral size of a lead or scintillator plate is  $109.7 \times 109.7 \text{ mm}^2$ . Each plate has 144 holes equidistantly arranged in a  $12 \times 12$  matrix, in which the spacing between the holes is 9.3 mm. The diameter of the holes is 1.3 mm, both in the lead and the scintillator plates. Inserted into the holes are 72 WLS fibers, with each fiber looped at the front of the module so that both ends of a fiber are viewed by a photo-detector. Such a loop (radius  $\sim 2.5 \text{ cm}$ ) may be approximated by a mirror with a reflection coefficient of about 95% [10]. The fiber ends are collected in one bunch, squeezed, cut and polished, and connected to a photo-detector through a small air gap. The complete stack of all plates is held in compression by four 1-mm stainless steel wires. The module is wrapped with 150- $\mu\text{m}$  TYVEK paper which has light reflection efficiency of about 80%.

The mechanical parameters of the module are summarized in Table 1.

The module is assembled in a special assembling berth that allows one to subject the assembled modules to cyclic longitudinal loadings up to 800 kg. This procedure prevents subsequent longitudinal shrinkage of the assembled modules and provides long-term stability for the length of the module to an accuracy of  $\simeq 1 \text{ mm}$ .

Table 1

Parameters of the improved Shashlyk module.

Transverse size	$110 \times 110 \text{ mm}^2$
Scintillator thickness	1.5 mm
Spacing between scintillator tiles	0.350 mm
Lead absorber thickness	0.275 mm
Number of the layers	300
WLS fibers per module	$72 \times 1.5 \text{ m} = 108 \text{ m}$
Fiber spacing	9.3 mm
Hole diameter (lead/scint.)	1.3 mm
Diameter of WLS fiber (Y11-200MS)	1.0 mm
Fiber bunch diameter	14.0 mm
External wrapping (TYVEK paper)	150 $\mu\text{m}$
Effective radiation length, $X_0$	34.9 mm
Effective Moliere radius, $R_M$	59.8 mm
Effective density	2.75 $\text{g}/\text{cm}^3$
Active depth	555 mm (15.9 $X_0$ )
Total depth (without photo-detector)	650 mm
Total weight	21 kg

## 2.2 Improvements of the Module Geometry

The mechanical construction of the module was revisited to minimize the insensitive area, to increase the effective radiation density, and to improve the sampling ratio and transverse light collection uniformity.

An important innovation in the mechanical design of the module is the “LEGO”-type locks for the scintillator tiles shown in Fig. 1. These locks, four per tile, maintain the position of the scintillators and the 350- $\mu\text{m}$  gaps, providing sufficient room for the 275- $\mu\text{m}$  lead tiles without optical contacts between lead and scintillator. This mechanical structure enables removal of the 600 paper tiles that were in earlier modules, and allows reduction of the diameter of the fiber holes to 1.3 mm and removal of the compressing steel tapes at the sides of the module. Compared to the earlier Shashlyk module, the holes/cracks and other insensitive areas were reduced from 2.5% to 1.6%, and the module’s mechanical properties such as dimensional tolerances and stiffness were significantly improved. By removing the paper tiles, the effective radiation length could be reduced from 4.0 cm to 3.5 cm.

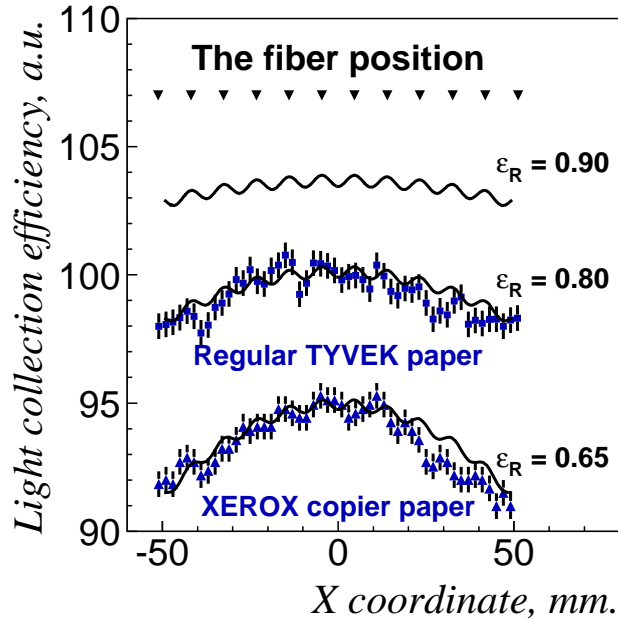


Fig. 3. The dependence of the light collection efficiency in the scintillator tile on the  $x$ -coordinate of the point-like light source. Solid lines are the simulations for the specified reflection efficiencies  $\varepsilon_R$  of the wrapping material.

The sampling, i.e., the relation between thicknesses of lead and scintillator tiles, dominates in the energy resolution of the Shashlyk module. However, one has only limited ability to improve the “pure” sampling contribution to the energy resolution of the Shashlyk module. Decreasing the thickness of the lead will increase the length of the module, while the proportional decreasing both the lead and scintillator thicknesses will reduce the light collection efficiency. Nevertheless, by removing the paper between the lead and scintillator tiles, both the sampling could be improved and the length of the module could be shortened. Compared to the design of the previous module [3], the sampling ratio was improved by a factor of 1.25.

The dominant source of non-uniformity of the light collection is the absorption of light at the edges of a scintillator tile. The reflection efficiency on the edges of the scintillator tile is crucial. In the new module, the WLS fiber density was effectively increased by reducing the size of the tiles to 10.97 cm. This allows the outer fibers to be closer to the edge of the scintillator tile than they were with the “uniform” size of 11.16 cm for 12 fibers with 0.93-cm spacing. In addition, the module was wrapped with TYVEK paper (reflection efficiency about 80%). As a result, the light collection efficiency at the edges of the scintillator tile is only 2.3% smaller than in the center of the tile for the point-like light source. In the case of a 250-MeV photon shower, the difference is only 0.5%, which is negligible compared to the energy resolution of about 6% for such photons.

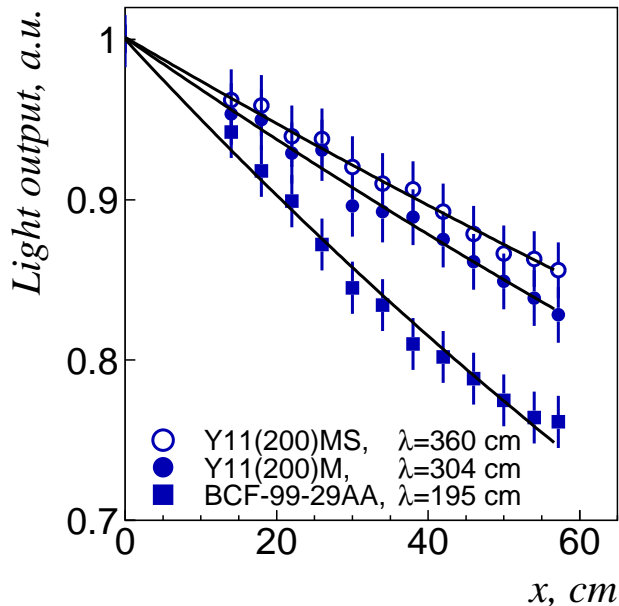


Fig. 4. The effective attenuation of the light in the fibers of Shashlyk module. Experimental data (marks) are fit by the exponential dependence  $\exp(-x/\lambda)$  (solid lines), where  $x$  is the distance to the photo-detector and  $\lambda$  is the effective attenuation length.

The experimental results for the light collection uniformity for TYVEK and Xerox copier papers are presented in Fig. 3. The measurements were made with a scintillator tile exposed to collimated  $^{90}\text{Sr}$  electrons. For comparison, the simulated light collection efficiencies are shown. One can see that there is consistency between the optical simulations and measurements. Further improvement could be achieved if Millipore paper with reflection efficiency of 90% were used [11].

### 2.3 WLS Fibers

A main concern about the WLS fibers for the Shashlyk readout is the light attenuation length in a fiber. Longitudinal fluctuations of electromagnetic showers are about 3-4 cm (one radiation length). The effective attenuation length in fibers, including the effect of the fiber loop and the contribution of the short-distance component of light, must be greater than 3-4 m to have this contribution to the energy resolution be much smaller than the sampling contribution.

We have measured (see Fig. 4) the light attenuation in few multi-clad WLS fibers using a  $1 \times 1 \text{ cm}^2$  wide muon beam penetrating the module transversely.

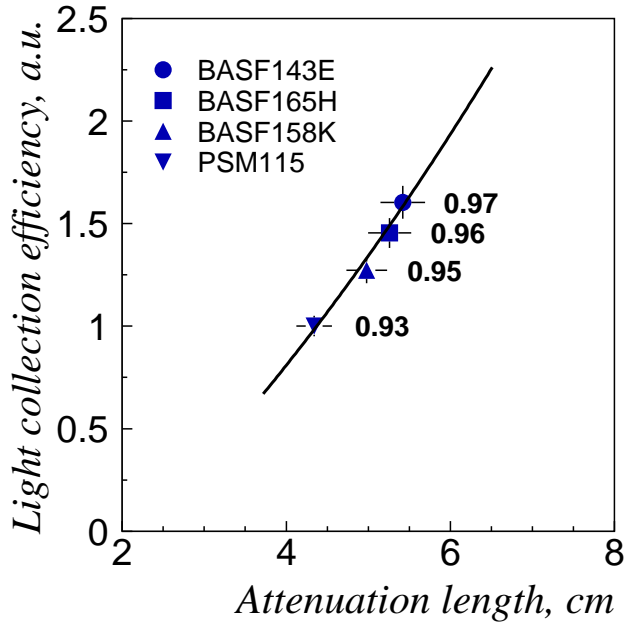


Fig. 5. The parametric dependence of the light collection efficiency on the effective attenuation length due to the reflection efficiency. The solid line is the result of a calculation based on the model of Ref. [3]. For each scintillator, the calculated reflection efficiency is displayed.

The effective attenuation length of 3.6 m in KURARAY Y11(200)MS fiber satisfies our requirements. In comparison with other fibers, this commercial fiber also provides the best reemission efficiency of blue scintillation light, and has excellent mechanical properties, high tensile and bending strength, and high uniformity in cross-sectional dimensions. For example, its light reemission efficiency is a factor of 1.5 larger than that for any Bicron WLS fiber, and the diameter for any round fiber is more uniform than others in that it varies by no more than 2.0%.

#### 2.4 Scintillator

An important contribution for the improvement of the photo-statistics over earlier designs of Shashlyk modules is the use of new scintillator tiles with an increased light collection efficiency. An optimization of the light yield of the scintillator tiles for the KOPIO Shashlyk modules has been developed and carried out at the IHEP scintillator facility (Protvino, Russia) [9]. In the previous Shashlyk calorimeters, scintillator based on PSM115 polystyrene was used. The new modules employ BASF143E-based scintillator.

Though there is no actual increase in the amount of light produced by a charge



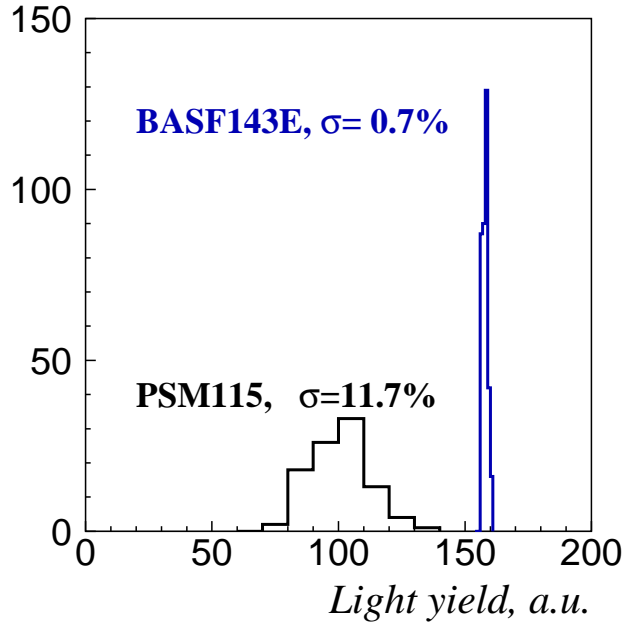


Fig. 6. Comparison of the light-yield spread for scintillator tiles used in earlier (PSM115) and new (BASF143E) Shashlyk modules.

particle, the light collection efficiency in the new scintillator tile has a gain by a factor of 1.6. Because the index of refraction for the polystyrene-based scintillator is 1.59, only light from total internal reflection on the large side of the scintillator tile can be captured by a WLS fiber. The total internal reflection efficiency can potentially be as large as 100%. However, this value is not reachable for realistic surfaces. Many reflections usually occur before light is captured and re-emitted by a WLS fiber. Both the effective attenuation length and the light collection efficiency in a scintillator tile depends on the light reflection efficiency. As shown in Fig. 5, the parametric dependence of the light collection efficiency on the attenuation length, calculated from our model of module optics [3], is in a good agreement with the experimental results.

The new plastic base of the scintillator material and the new production technology of tiles yields a 97% reflection efficiency from the scintillator surface, and strongly improves the reproduction quality (see Fig. 6) of the tiles. The latter is crucial for good longitudinal light collection uniformity. Due to the fluctuation of the depth of the electromagnetic shower in the calorimeter module, good reproduction quality of the tiles is a mandatory condition for an appropriate performance of the  $3\%/\sqrt{E}$  (GeV) module.

Fluors for the new scintillator composition, BASF143E polystyrene + 1.5% PTP + 0.04% POPOP were selected [12,13] to match well with the absorption spectrum of the Kuraray Y11(200)MS WLS fiber (Fig. 7). With a BASF143E-based scintillator and KURARAY fibers, the effective light yield in the KOPIO

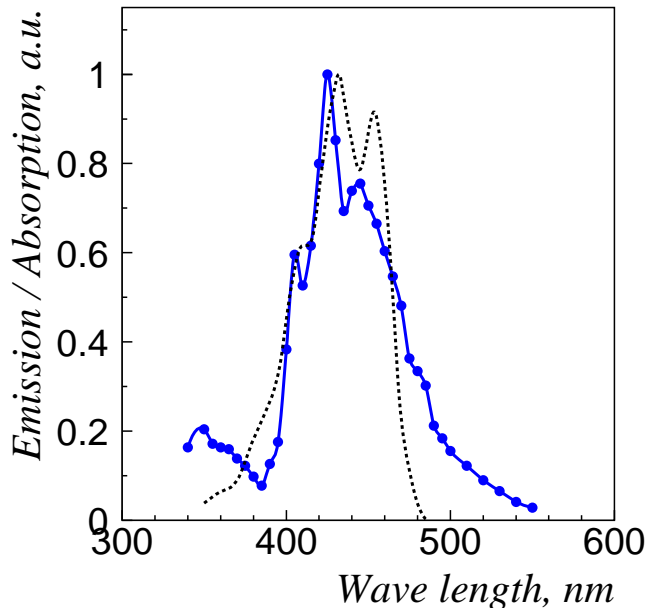


Fig. 7. The closed circles and solid line are the measured emission spectra of the BASF143E-based scintillator. The dashed line is the absorption spectrum of KURARAY Y11(200)MS WLS fibers.

Shashlyk module (at the entrance to the photo-detector) becomes  $N_\gamma \approx 60$  photons per 1 MeV of the incident photon energy.

The radiation hardness of the scintillator may be a limiting factor for using the Shashlyk calorimeter in the modern high statistics experiment. It was reported [12] that the radiation stability of BASF143E-based scintillator is a dose level 120 krad, and the recovery time is about 80 days. This limitation would not be a problem for the KOPIO Calorimeter for which this Shashlyk module was designed.

## 2.5 Photo-detector

The Avalanche Photo Diode, a detector with high quantum efficiency, provides another important improvement of the photo-statistics contribution to the energy resolution of the Shashlyk module.

Our previous experimental studies of fine-sampling Shashlyk modules [3] have shown that the performance of Shashlyk calorimeter modules with photomultiplier (PMT) readouts agrees with the simulations and nearly satisfies the requirements formulated in the introduction. However, these test measurements were made in an optimal environment for PMT readout: no magnetic

Table 2

Some experimental and catalog parameters of large-area APDs. Quantum efficiency is given for green light,  $\lambda = 500$  nm. Signal rise and fall time are measured without amplifier. Excess noise factor, which approximately depends on the gain  $M$  as  $2+kM$  is given for  $M = 100$ .  $I_S$  and  $I_B$  are components of the dark current  $I_d = I_S + I_B M$ . The gain dependences on temperature,  $T$ , and high voltage,  $V$ , are given for  $M \sim 100$ . For RMD APD, we have observed a significantly different results for values of series resistance (and consequently for signal fall time) which is indicated in the Table.

Manufacturer	API	RMD	EG&G	Hamamatsu
Model number	630-70-74-510	S1315	C30703E	S8664-1010N
Active area, mm <sup>2</sup>	200	169	100	100
	∅16	13 × 13	10 × 10	10 × 10
Quantum Eff., %	94	65	75	80
Capacitance, pF	130	110	80	270
Series resistance, Ω	15	50(280)	10	< 5
Signal rise time, ns	6	9	5	4.4
Signal fall time, ns	16	24(80)	15	25
Gain	≤ 600	≤ 1000	≤ 200	≤ 300
Excess noise factor	2.2	2.05	3.2	2.5
$I_S$ , nA	50	310	90	3
$I_B$ , nA	0.6	3.8	0.4	0.3
$\frac{dM}{M dT}$ , °C <sup>-1</sup>	-0.03	-0.03	-0.04	-0.045
$\frac{dM}{M dV}$ , V <sup>-1</sup>	0.014	0.016	0.03	0.03

fields, short measuring runs, and continuous and stable electron beams.

These conditions do not properly represent those that would be encountered in the KOPIO experimental environment. Our main concern is related to the leakage of the magnetic field from the downstream magnet of up to 500 Gauss. Another serious problem is the cycling of real beam every several seconds, with possible significant variations in intensity. This will produce short- and long-term variations of the PMT gain, which will destroy the response stability of the detector performance. In addition, the quantum efficiency of PMTs, even for the best “standard” green-sensitive tubes, e.g. PMT 9903B of Electron Tube Inc., is relatively low, about 20% at 500 nm (the region of WLS-fiber response).

Consideration was thus given to alternative photo-detectors. Recent progress in the development of new APDs with large active areas (up to 200 mm<sup>2</sup>),

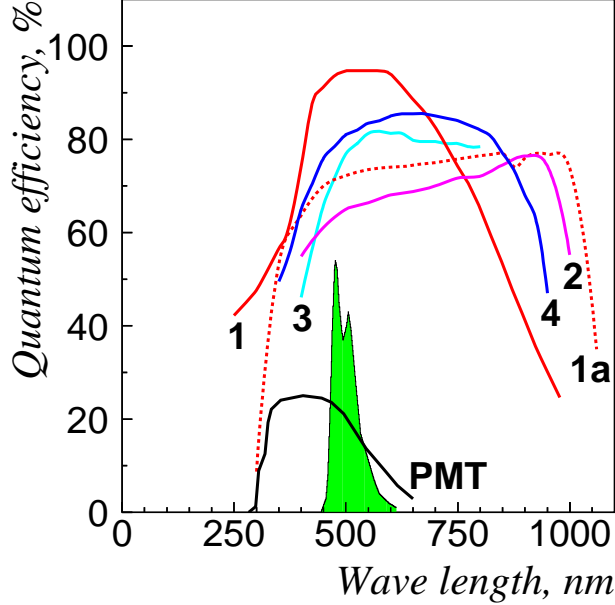


Fig. 8. The quantum efficiency of considered APDs: 1– API ( $\text{SiO}_2$  window), 1a– API (epoxy window), 2– RMD (epoxy window), 3– EG&G ( $\text{SiN}_x$  window), 4– Hamamatsu (epoxy window). For comparison, quantum efficiency of the 9903B PMT is also shown. The histogram is an emission spectrum of the Kuraray Y11200MS WLS fiber.

low capacitance, low dark current, high gain (up to 1,000), and high quantum efficiency (up to 90%) allows us to consider these photo-detectors as primary candidates for the improved Shashlyk Calorimeter. We have studied the large area ( $\geq 100 \text{ mm}^2$ ) APDs of (i) *Advanced Photonix Inc.* (API), (ii) *RMD Instruments Inc.* (RMD), (iii) *Perkin-Elmer Inc.* (EG&G), and (iv) *Hamamatsu Photonix K.K.* Some characteristics of these APDs are summarized in Table 2. Here, we briefly report the results of our study.

- Size of the active area.  
The fibers from the Shashlyk module, described in this paper, are collected in a 14 mm diameter bunch. This size is well matched to the API APD, which has a diameter of 16 mm. Optical light guides must be used with other APDs that were considered, to match the size of the active area. For  $10 \times 10 \text{ mm}^2$  active area, this will result in a light loss of at least 10-15%.
- Response uniformity of the active area.  
This feature is important for the Shashlyk module because each fiber delivers light to only a small part of the total sensitive area. The response of the selected APD varies by less than 3% over the active area. Usually, PMTs exhibit poor spatial response uniformity ( $\geq 20\%$ ).
- Quantum efficiency of the sensitive area.  
Photo-statistics, directly dependent on the quantum efficiency ( $Q$ ) of the

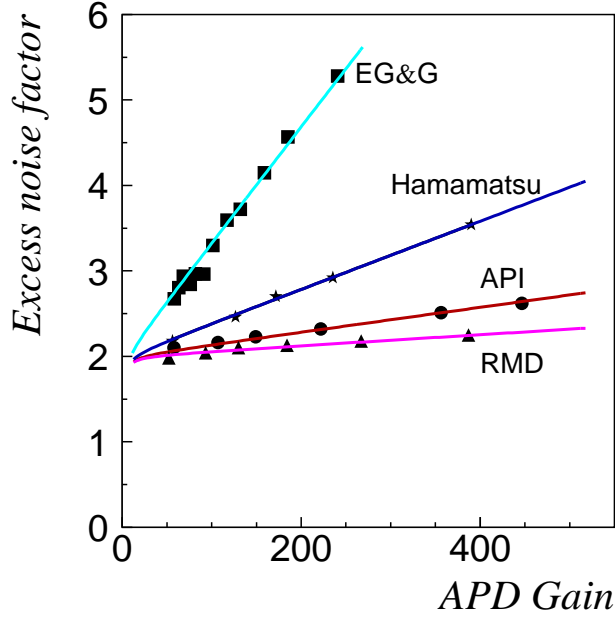


Fig. 9. The APD excess noise factor *vs.* the APD gain.

photo-detector, is an important contribution to the energy resolution of a calorimeter. For green light emitted by Kuraray fibers, the APDs have much higher quantum efficiencies than PMTs (see Fig. 8). For example, the quantum efficiency of the API APD is 94%, a factor 5 higher than quantum efficiency of the 9903B PMT. It should be noted that the photo-statistics contribution depends also on the fluctuations of the photo-detector gain,  $(\sigma_E/E)_{\text{ph.stat.}}^2 = F/QN_\gamma$ , where  $F$  is the so-called excess noise factor and  $N_\gamma$  is the number of primary photons at the entrance of the photo-detector. For an ideal photo-detector,  $F = 1$ , for a high-linearity PMT it is usually between 1.3 and 1.6. For an APD, excess noise factor dependences on gain  $M$  may be well approximated as  $F \simeq 2 + kM$  if  $M \geq 20$  [15]. The experimentally measured behavior of  $F$  versus  $M$  for the APDs under consideration is shown in Fig. 9. Taking into account both quantum efficiency  $Q$  and excess noise factor  $F$ , we conclude that API APD has best “photo-statistics quality” ( $Q/F \simeq 43\%$  ( $M_{\text{APD}} \simeq 100$ )) of about a factor 3.5 better than 9903B PMT.

- Electronic noise of the photo-detector/amplifier chain.  
In the case of a Charge Sensitive Amplifier (CSA) with a simple  $CR$ - $RC$  shaper, the contribution of the electronic noise from the photo-detector/amplifier chain to the energy resolution can be estimated as:

$$\sigma_{\text{noise}} = \frac{1}{n_\gamma Q} \sqrt{\frac{I_S/M^2 + I_B F}{q} \Delta t + \frac{\sigma_{\text{amp}}^2(C, \Delta t)}{M^2}} \quad (1)$$

where  $n_\gamma$  is number of photons at the entrance of photo-detector per unit of

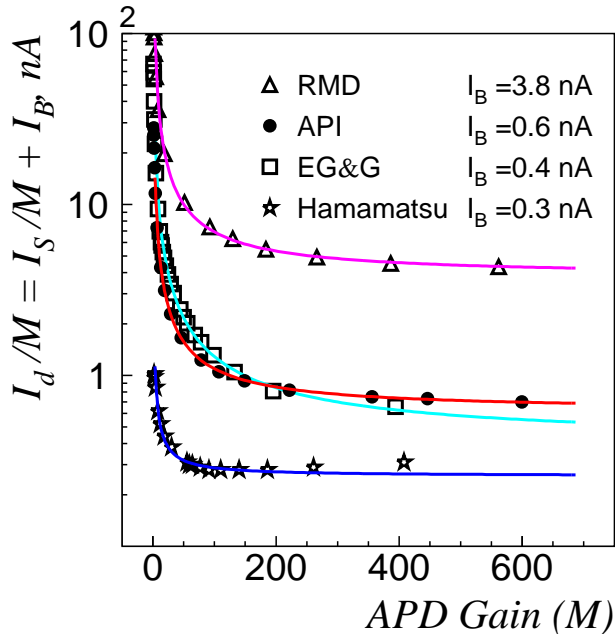


Fig. 10. The APD dark current.

the deposited energy ( $n_\gamma \approx 60 \text{ MeV}^{-1}$  for the improved Shashlyk module),  $q = 1.6 \cdot 10^{-19} \text{ C}$  is electron charge, and  $\Delta t$  is the measurement gate width. The photo-detector noise can be related to the  $I_S$  (surface leakage current) and  $I_B$  (bulk current), the components of the dark current  $I_d = I_S + I_B M$ . The amplifier noise,  $\sigma_{\text{amp}}$ , defined here as Equivalent Noise Charge (ENC) depends on the gate width  $\Delta t$  and the photo-detector capacitance  $C$ .

For a PMT readout, the photo-detector noise is negligible due to a small ( $\sim 0.1 \text{ nA}$ ) PMT dark current and big ( $\geq 10^5$ ) gain. The experimentally measured behavior of the APD dark current versus gain  $M$  for our APDs is shown in Fig. 10. The contribution of  $I_S$  to the noise becomes negligible if  $M \geq 100$ . For the API APD, the photo-detector contribution to the noise can be estimated as  $0.5 \text{ MeV}$  for  $\Delta t \approx 100 \text{ ns}$ ,  $M \geq 100$ , and environmental temperature  $T = 25 \text{ }^\circ\text{C}$ .

The value of the amplifier noise  $\sigma_{\text{amp}}$  is usually measured experimentally. We have used a fast low noise CSA, that has been designed for KOPIO Calorimeter to optimize the signal-to-noise ratio and double-pulse resolution. Its charge-sensitive part was designed as a cascade amplifier with two parallel-connected low capacitance JFET transistors. We considered the Russian KP341A and Japanese SK2394/YJ5 transistors for this amplifier. Both transistors are characterized by a high transconductance ( $g_m > 20 \text{ mA/V}$ ) for moderate noise current and low input capacitance ( $C_{\text{JFET}} < 10 \text{ pF}$ ). For a  $100 \text{ ns}$  gate, the ENC dependence on the photo-detector capacity  $C$  (pF) was measured to be  $270 + 18.8C$  for the KP341A and  $500 + 10.9C$  for the SK2394/YJ5. We used an amplifier with two SK2394/YJ5 transistors in the test beam measurements. For the API APD

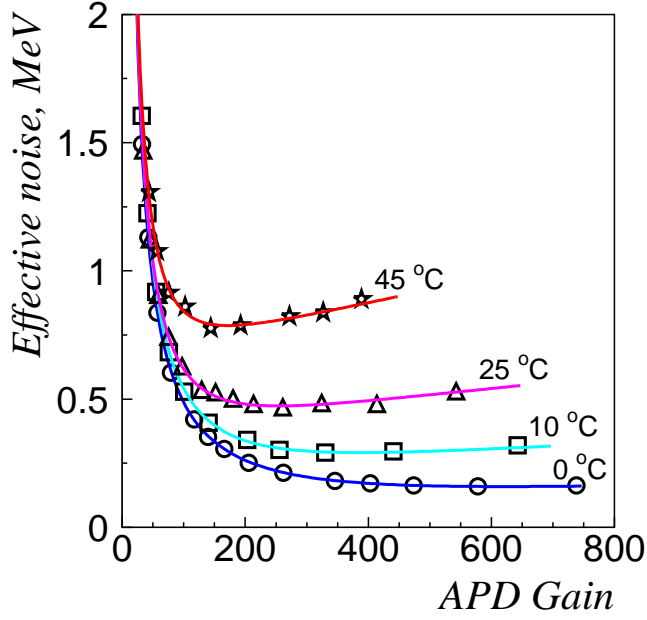


Fig. 11. Effective noise of the API APD/amplifier chain *vs.* the APD gain for various environmental temperatures.

( $C = 130$  pF) the amplifier noise may be estimated as 0.3 MeV resulting in a total photo-detector/amplifier chain noise of 0.6 MeV for  $\Delta t = 100$  ns,  $M = 100$ , and  $T = 25$  °C. It should be underlined, that large photo-statistics,  $n_\gamma$ , is a crucial factor in achieving required effective noise suppression.

- Gain and noise dependence on the temperature.

The APD performance is very sensitive to the environmental temperature. Because  $\frac{1}{M} \frac{dM}{dT} \simeq -4\%$ , temperature and gain monitoring is important in using APDs in the experiment. For the API APD, the noise dependence on temperature is shown in Fig. 11. A thermostable cooling system and appropriate increase of the APD gain may allow one to lower the effective noise down to the level of 0.2-0.3 MeV.

- Gain dependence on High Voltage.

According to our experimental study,  $\frac{1}{M} \frac{dM}{dV} \approx (2 - 3)\%$  depending on the environment temperature and APD gain. The dependence is similar to those of PMTs.

- Gain dependence on the rate.

Contrary to PMTs, there is almost no dependence of APD gain on rate. In our test measurements with API APDs, we did not find any gain variations for the rates up to few MHz. However, APDs are used with preamplifiers. For slow preamplifiers, there may be a rate dependence due to the pile-up.

- Time response of the API APD.

The time response of the API APD (without amplifier) to a short-duration (3 ns) light pulse with an intensity corresponding to a 700-MeV photon, is

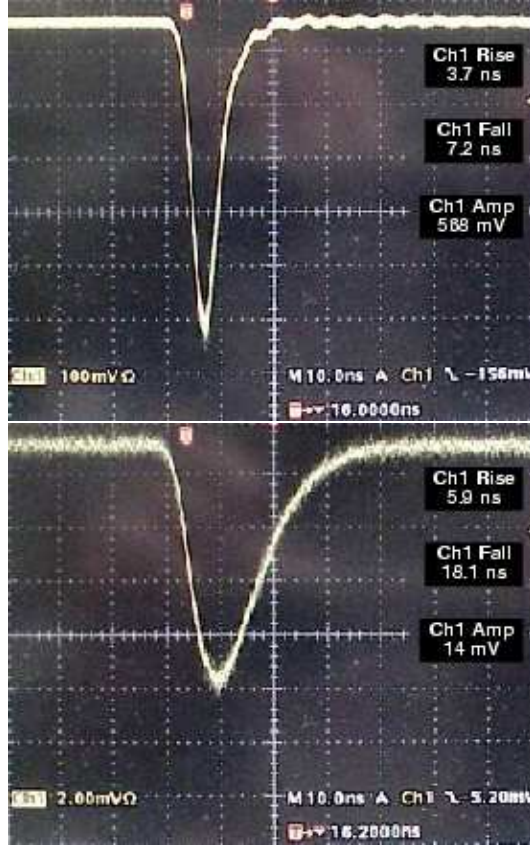


Fig. 12. PMT-9903B (upper) and API APD (lower) responses to short, 3 ns, light pulses. The intensity of the light pulse corresponds to the 700 MeV photon signal.

shown in Fig. 12. The APD rise time of 5.9 ns is comparable with 3.7 ns for the 9903B PMT response to the same light pulse. Due to higher APD capacitance, the fall time of the APD pulse, 18.1 ns, is longer than that for the PMT response of 7.2 ns.

The difference between a PMT and an APD time response becomes less important if we take into account the Shashlyk module signal (light pulse) duration. (see Fig. 18). However, both the photo-detector capacitance  $C$  and serial resistance  $R_s$  are important parameters for the time response of the APD.

- Operation in magnetic field.

As opposed to PMTs, APDs can operate in a magnetic field of up to 80 kG [14].

From the above consideration of the available APDs, we conclude that the Advanced Photonix Inc. APD 630-70-74-510 is the optimal choice for our goals. Having the largest active area which matches well with the fiber bunch size, this commercial APD has best photo-statistics quality,  $Q/F$ , and sufficiently short time response when compared to other large area APDS . The relatively high gain and low dependence of excess noise factor on gain, allows us to optimize detector performance, e.g., to reduce the effective photo-



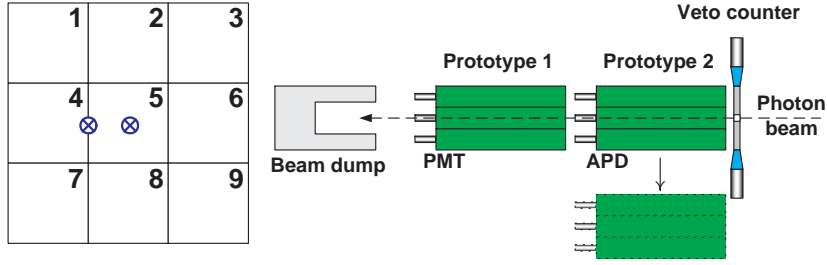


Fig. 13. Schematic drawing of the detector setup. An indexing of the nonet modules and a beam position at a studied nonet for the energy, inefficiency (center), and timing (between modules 4 and 5) measurements is shown on the left.

detector/amplifier noise to the 0.2-0.3 MeV level for reasonable values of the environmental temperature.

These characteristics of the API APD together with the improved light yield in the new Shashlyk module reduces the photo-statistics contribution to the energy resolution of the calorimeter to a negligible level of  $0.7\%/\sqrt{E}$  (GeV). The electronic noise contribution is also negligible.

### 3 Experimental Study of the Calorimeter Prototypes

#### 3.1 Test beam

Test measurements of the prototype of a Shashlyk calorimeter with energy resolution of  $3\%/\sqrt{E}$  (GeV) have been made with the photon beam from the Laser Electron Gamma Source (LEGS) facility [16]. LEGS is located at the National Synchrotron Light Source (NSLS) at Brookhaven National Laboratory. A continuous photon beam with an energy range of 150 to 400 MeV is produced by laser photons Compton backscattered by 2.58-GeV storage ring electrons. The energy of each backscattered photon was known by detecting the Compton scattered electron.

The tagged photon beam had an average intensity of  $\sim 3 \times 10^5$  Hz, horizontal and vertical sizes of  $\sim 1.5$  cm at the detector position, and an angular spread of  $\sim 2$  mrad. The photon energy was tagged with an accuracy of  $\delta E_\gamma/E_\gamma \approx 1.5\%$ . The timing accuracy of the tagging spectrometer was  $\simeq 1$  ns. Several monochromatic photon energy lines in the range of 220 MeV to 370 MeV were triggered in our measurements.

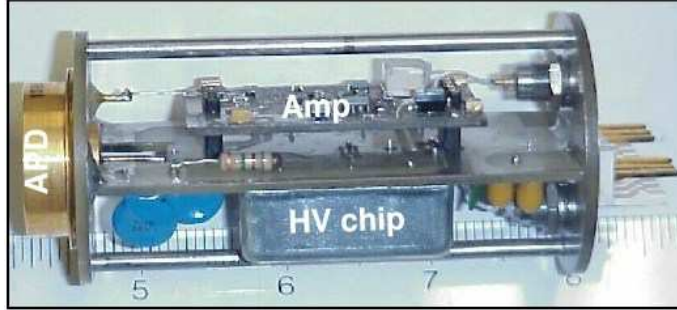


Fig. 14. View of an APD unit.

### 3.2 Calorimeter Prototypes

Two arrays of  $3 \times 3$  prototype modules with the same sampling of  $275 \mu\text{m}$  of lead and 1.5 mm of scintillator were tested as shown in Fig. 13.

The first array (prototype 1) contained 9 module with paper between lead and scintillator (earlier design) with the 30-mm-diameter, green-sensitive PMT-9903B of *Electron Tube Inc.*

The second array (prototype 2) contained a nonet of new design modules equipped with the 16 mm diameter API APD. The APD detector housing, an instrumented unit including the APD itself, the APD amplifier, and the APD HV bias, is shown in Fig. 14.

Because the new Calorimeter photo-detector (APD) draws a typical photocurrent of less than 0.1 mA, an economical way to build the Calorimeter HV system is to develop an active, compact individual HV-unit mounted directly into each APD housing. This kind of HV system eliminates expensive and bulky HV cables and connectors, lowers the power consumption per individual power supply, and reduces the electrical HV hazard associated with traditional HV supplies.

In the test measurements, two types of APD HV supplies were tested: traditional HV supply: a NIM standard *BERTAN 377P*, and a HV “built-in” unit (see Fig. 14) with a new commercial, compact, regulated and programmable LV-HV converter (C20), produced by EMCO. The stability of both bias systems was better than 0.1 V/hour, which provided an APD gain stability better than 0.3%.

### 3.3 Cooling

The photo-detectors (APD) of the Prototype 2 were placed in a thermo-isolated cooling unit. During the test period of 20 hours, the APD temperature was kept at 18 °C. Variation did not exceed 0.2 °C. Such cooling system allowed us to neglect the temperature dependent effects in data analysis.

### 3.4 Readout

One of the goal of the photon beam measurements was to test the readout prototype for the KOPIO experiment. The readout electronics had to be capable of measuring energies with a digitization uncertainty of 0.5 MeV in a dynamic range of 2–1000 MeV, and the time of arrival with respect to the beam micro-bunch clock with an uncertainty of less than a few hundred ps. Operation of this readout electronics was required to be completely pipelined with no dead time. It also had to be capable of forming and discriminating the total energy signals and the total number of hits in the Calorimeter. To meet these performance requirements for energy and timing resolution with PMTs or APDs, in an economical way, we have investigated using Wave Form Digitizers (WFDs). Our WFD was based on an 8-bit 140-MHz WFD which has been developed by Yale University [17]. Its measurements were compared with those of conventional 12-bit LeCroy QDCs.

### 3.5 Calibration and Monitoring

The energy resolution of  $\sim 3.0\%/\sqrt{E}$  requires that a pre-calibration and monitoring system be developed.

We have used vertical cosmic-ray muons for pre-calibration of the calorimeter prototypes, as we did in Experiment E865 [4]. The accuracy of this pre-calibration was estimated to be about 4%.

To monitor prototype performance during our measurements and to correct the variation of the photo-detector gains with an accuracy of 0.4%, we have used a prototype of the KOPIO Calorimeter monitoring system. This system employs high-brightness Light Emitting Diodes (LEDs NSPB-310A) to inject blue light into the scintillator via a clear fiber (see Fig. 1). Stabilization of the LED light was obtained by means of an optical feedback provided by a PIN photo-diode as shown in References [18] and [19].

This system satisfied a number of our specific requirements:

- short light pulse duration, less than 15 ns;
- variable light pulse intensity (5,000–20,000 photons/channel);
- variable pulse repetition rate (up to 1MHz);
- high long-term and short-term temperature stability, better than 0.1%;
- small variation in the flash amplitude, less than 0.2%.

The monitoring system can also serve as a pre-calibration of the module readout chain at the 10% level.

For final calibration of the prototypes we used the photon beam. Both calorimeter prototypes were mounted on platforms that could be moved horizontally and vertically with respect to the beam line, so that each prototype module could be calibrated (with an accuracy  $\leq 1\%$ ) by using the 250-MeV photon beam that passed through the central region of the module at normal incidence.

## 4 Experimental Results

### 4.1 Calorimeter prototype response

The pedestal response, the sum of electronic noise and pile-up for individual modules, was measured during the test runs by using a special gate signal that was shifted from the photon timing by up to 1  $\mu$ s. The contribution of this effective noise to the energy resolution was  $(0.5 \pm 0.1)$  MeV for the case of the “APD+QDC” readout. The total equivalent noise for the “APD+WFD” readout was  $(1.0 \pm 0.2)$  MeV. This latter value is twice as large as that for the first one due to a digitization uncertainty of the 8-bit WFD. The lowest equivalent noise,  $(0.2 \pm 0.1)$  MeV, was obtained with the PMT-9903B tubes.

The typical response of the nonet of the “APD+WFD”-instrumented modules to a 340 MeV photon hitting the nonet at the center of the central module, is shown in Fig. 18. The measured signal distribution in the WFD was fit by a function  $Af(t - t_0) + P$ , where  $f(\tau)$  is an experimentally determined pulse shape function. The signal amplitude  $A$ , signal time  $t_0$ , and pedestal  $P$  were free parameters in the fit.

### 4.2 Energy Resolution

The energy resolution was measured for both prototypes 1 and 2. The photon beam was directed to the center of the module nonets. Energy spectra of 250- and 370-MeV photons in the Shashlyk nonet with the APD+WFD

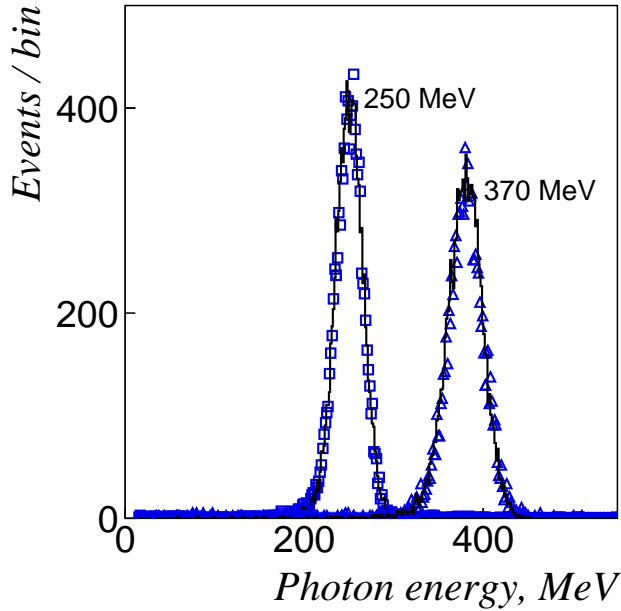


Fig. 15. Comparison of the experimental (marks) and simulated (solid lines) energy spectra in the Shashlyk prototype with APD+WFD readout.

readout are shown in Fig. 15. Note the good agreement between Monte-Carlo and experimental distributions, that gives us a confidence that our simulation model, which includes effects of the beam energy spread, energy loss upstream calorimeter, photon shower evolution, light collection in scintillator tiles and light transmission in WLS fibers, the response of the photo-detector, and noise of the entire electronic chain, properly reproduces the actual calorimeter response.

The energy-resolution results for various readouts are displayed in Fig. 16. The best result was achieved for the “APD+WFD” readout. A fit to these experimental data gives

$$\sigma_E/E = (1.96 \pm 0.1)\% \oplus (2.74 \pm 0.05)\%/\sqrt{E \text{ (GeV)}}, \quad (2)$$

where  $\oplus$  means a quadratic summation. The relatively large constant term of 2% may be explained by the short,  $15.9\text{-}X_0$  radiation length of the module. The constant term may be improved by increasing length of the module. However, this term is not essential for the photon energy range of 50–1000 MeV.

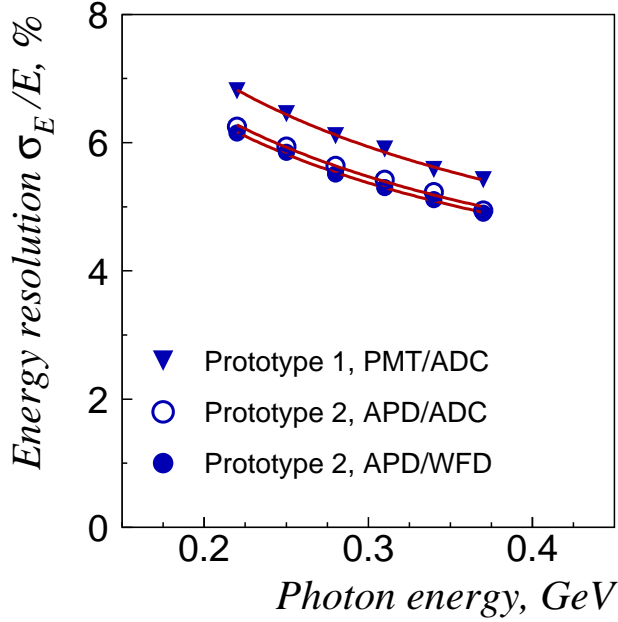


Fig. 16. Energy resolution of a prototype of the Shashlyk Calorimeter.

### 4.3 Time Resolution

To estimate the time resolution, we measured the time difference for the signals produced by the same shower in two neighbor modules. By using this measurement technique, the 340 MeV photon beam was directed between central module (#5) and left module (#4), see Fig. 13.

Only events with the full photon energy ( $E_4 + E_5 = 330 \pm 20$  MeV) deposited in these two modules were selected for analysis. The dependence of the time difference variance on the energy deposited in module #4 is shown in Fig. 17. The time difference resolution drops significantly if one of the two deposited energies is close to zero or, alternatively, if one of the energies is close to 330 MeV and the other is necessarily close to zero. Assuming that both modules have the same time resolution, we have obtained from Fig. 17

$$\sigma_T = \frac{(72 \pm 4) \text{ ps}}{\sqrt{E \text{ (GeV)}}} \oplus \frac{(14 \pm 2) \text{ ps}}{E \text{ (GeV)}} \quad (3)$$

The signals we use to evaluate the time resolution are strongly correlated because they are produced by the same electromagnetic shower. This may result in a wrong value of the time resolution. For example, the contribution of the longitudinal fluctuation of the shower is suppressed in such measurements. To ensure that our test-beam result does not underestimate the actual time

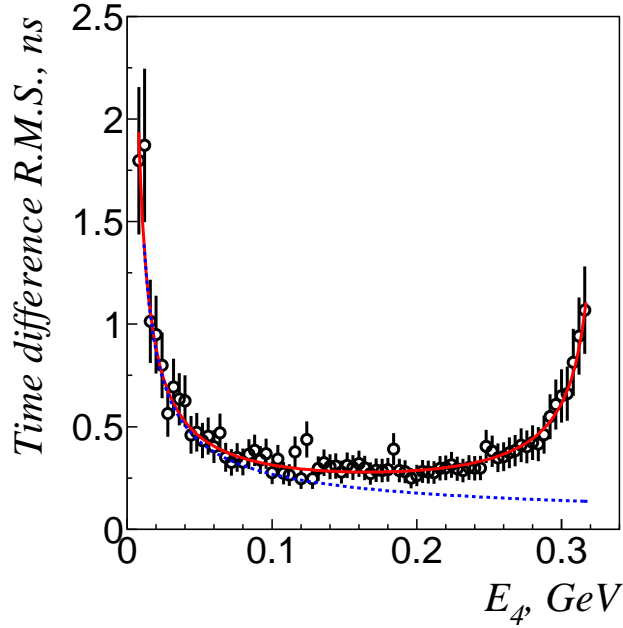


Fig. 17. Experimental evaluation of the time resolution of a Shashlyk module (see text for details).  $E_4$  is energy measured in module #4. Solid line is an expectation of the time difference R.M.S.  $\sigma_{(T_4-T_5)}(E_4) = \sqrt{\sigma_T^2(E_4) + \sigma_T^2(0.33 - E_4)}$ , where  $\sigma_T(E) = 0.072/\sqrt{E} \oplus 0.014/E$  (shown by dashed line) is a fit-estimated time resolution in each module, #4 and #5.

resolution, we carried out a Monte Carlo simulation of the time resolution.

To simulate the time response and time resolution of a Shashlyk module, a Monte Carlo model was upgraded for the evolution of the light signal in a module. Ionization produced by a charged particle in a scintillator tile survives several transformations before the corresponding light signal appears at the entrance of a photo-detector. Ionization produced by an electromagnetic shower occur at different space points and different times, resulting in a time spread of the photo-electron emission in the photo-detector. In addition, the actual emission delays depend randomly on the decay times in the scintillator and the WLS fibers, light collection time in the scintillator fiber, and the propagation of light in the WLS fiber. The following effects have been taken into account in the model:

- the space-time distribution of hits in the Shashlyk module scintillator;
- the decay time in scintillator;
- the light collection time in the scintillator tile;
- the decay time in WLS fibers;
- the effective velocity of light propagation in WLS fibers;
- the light attenuation length in WLS fibers;
- bending loss in the WLS fiber loop; and

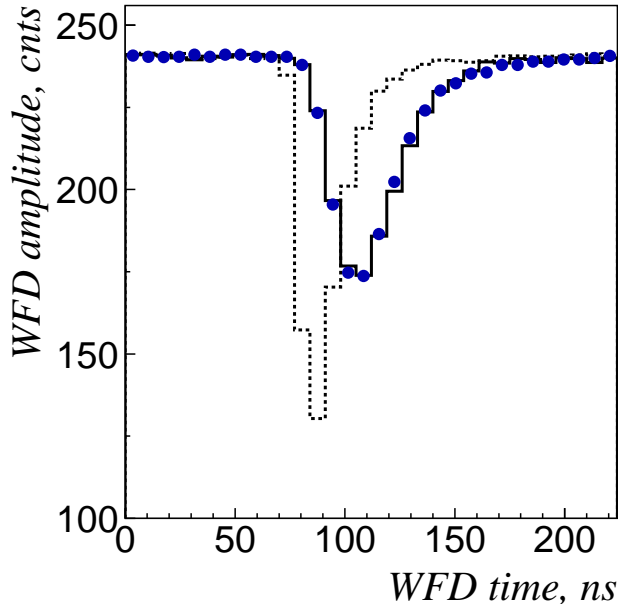


Fig. 18. A 340 MeV photon signal in WFD. Closed circles are experimental data. Solid line is the simulation, including readout chain response function. Dashed line is the light pulse shape at the entrance of the APD.

- the response function of the detector chain, including photo-detector (APD), preamplifier, cables and WFD.

The simulated response of the Shashlyk module for the 340 MeV photons is shown in Fig. 18. The shape of the simulated signal in a Wave Form Digitizer matches well an experimentally measured signal.

In the Monte-Carlo simulation of our time resolution measurements, we have obtained  $\sigma_{T_4-T_5} = 280$  ps if  $E_4 \approx E_5$  which is in a good agreement with the experimental value of 285 ps (see Fig. 17).

The Monte-Carlo simulations of the mean measured time and time resolution dependence on type of particle and its energy is shown in Fig. 19. To understand the behavior of mean time values we should note that by fitting the signal shape in a WFD we actually measure the center of gravity of the signal time distribution.

The main contributions to the relative signal delay are electron/photon tracking time before the hit and time of light propagation in the fiber. The average of time delays in both ends of the fiber does not depend on the actual position of the hit if we can neglect the light attenuation in the fiber. In such an approximation, the relative delay of the measured hit is solely defined by the time at which this hit occurred. In other words, the deeper shower pene-



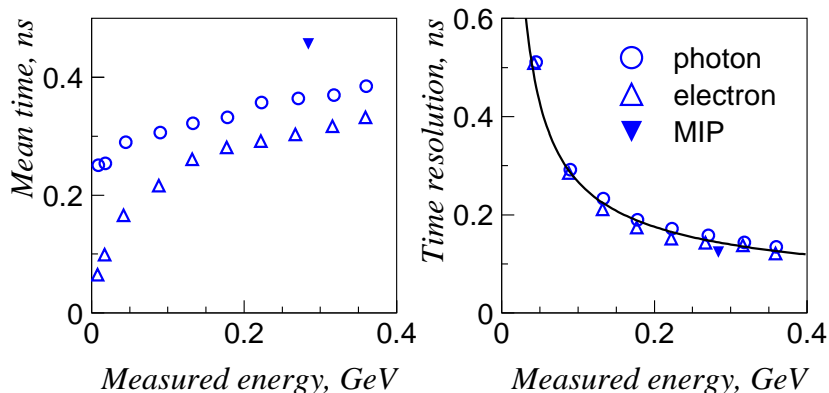


Fig. 19. Results of a Monte Carlo simulations of the time resolution of the Shashlyk module for photons, electrons, and Minimum Ionizing Particles (MIP). The solid line corresponds to a  $0.072/\sqrt{E} \oplus 0.014/E$  (ns), an approximation of the time resolution from our test-beam measurements. The simulated dependence of the mean measured time on type of particle and its energy is shown on the left.

trates in a module the larger time delay is measured. Since photons interact more deeply in the module than electrons, the measured time for photons is expected to be about 100 ps larger than that for electrons of the same energy.

It is interesting to note that one can suppress the dependence of the measured time on the type of particle and its energy if the loss of light in the loop were equal to  $2v/(c+v) \approx 0.7$ , where  $c$  is the speed of light in vacuum and  $v$  is the effective velocity of signal propagation in fiber. However, such a degradation of the loop would reduce the photo-statistics by about 30%, and also the contribution to the shower longitudinal fluctuations will be increased.

According to the Monte-Carlo simulation, the Shashlyk module time resolution obtained by our method, based on the measurement of time difference in the neighbor modules, is consistent with the actual time resolution of photon/electron detection.

#### 4.4 Photon Detection Inefficiency

To estimate the photon detection inefficiency due to fiber holes, the prototype 1 was located behind the prototype 2 array. The absence of a signal in the front array, while the total photon energy was deposited in the second, was interpreted as a penetration of the photon through the first prototype without interaction, *e.g.* through a fiber hole. Photons of 250 MeV were directed onto the face of the first array. The measured dependence of the photon detection inefficiency on the incident angle of the beam is compared with the simulation in Fig. 20. The relatively coarse step in the measured angles does not allow us

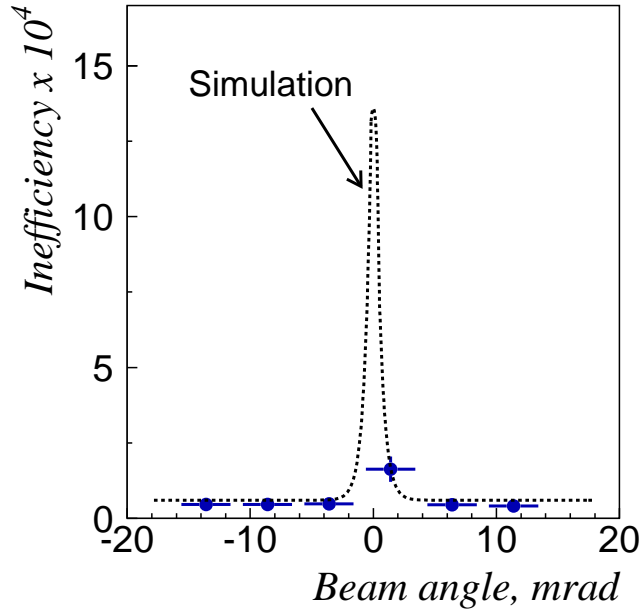


Fig. 20. The dependence of the photon detection inefficiency on the incident angle.

to accurately compare the experimental results with the simulation. However, our measurements clearly indicate that the effect of the WLS fiber holes is negligible if the incident angle is  $\geq 5$  mrad. For such angles, our experimental results agree well with the probability of photon interactions in about 8.25 cm of lead and 45 cm of scintillator. It has to be pointed out that the measurement of photon detection inefficiency in this way is insensitive to the photon “disappearance” in the Calorimeter, e.g. due to photo-nuclear reactions.

#### 4.5 Long-term APD Stability

To test the long-term stability of the photo-detector gain, the APD and PMT gains were monitored using LED signals over a 20 hour period. Experimental data resulting from this test are shown in Fig. 21. One can see a rate effect for the PMT-9903B after changing the photon beam intensity from 0 kHz to 300 kHz. No APD gain dependence on the photon beam intensity was observed after changing the photon beam rate over this range. The variation of the APD gain did not exceed 1%.

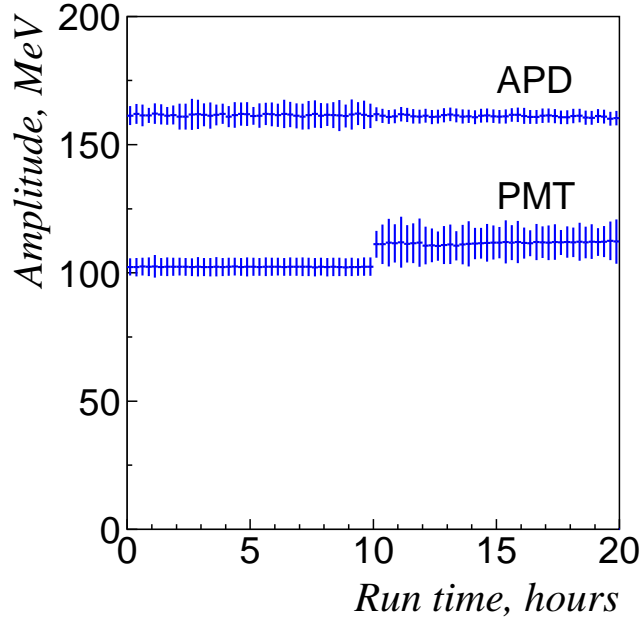


Fig. 21. Illustration of the long-term stability and gain dependence on the rate for the APD and PMT readout. The mean values of the LED signals were measured during 20 hours run. The 250 MeV, 300 kHz photon beam was switched from Prototype 2 with APD readout to Prototype 1 with PMT readout after 10 hours of the run. Vertical lines indicate the measured R.M.S. of the LED signal.

## 5 Summary

Modules for a Shashlyk Calorimeter with energy resolution

$$\sigma_E/E = (1.96 \pm 0.1)\% \oplus (2.74 \pm 0.05)\%/\sqrt{E \text{ (GeV)}}, \quad (4)$$

time resolution of

$$\sigma_T = (72 \pm 4 \text{ ps})/\sqrt{E \text{ (GeV)}} \oplus (14 \pm 2 \text{ ps})/(E \text{ (GeV)}), \quad (5)$$

and an inefficiency in photon detection due to the nature of the modules of

$$\epsilon \approx 5 \times 10^{-5} \quad (\Theta_{\text{beam}} > 5 \text{ mrad}) \quad (6)$$

have been constructed and experimentally tested. The characteristics experimentally determined for the Calorimeter prototype well meet the design goals of the KOPIO experiment.

To optimize the Calorimeter readout design, a Monte Carlo simulation model of the light transmission in scintillator tiles and WLS fibers, the response of the photo-detector, and noise of the entire electronic chain. This model accurately describes the experimental data.

## Acknowledgments

This work was supported in part by the US Department of Energy, the National Science Foundations of the USA and Russia. We thank the directorate of Institute for Nuclear Research (Moscow) and Institute for High Energy Physics (Protvino) for their support of this work. We are gratefully acknowledge all participants of the KOPIO Collaboration for numerous discussions of the Shashlyk Calorimeter performance. We are grateful to A. Sandorfi for the opportunity to use LEGS equipment in our test beam measurements. We are further indebted to E.N. Guschin, Yu.V. Musienko, and P. Rehak for many valuable discussions and suggestions.

## References

- [1] G.S. Atoyan, *et al.*, Nucl. Instr. and Meth, A **320**, 144 (1992).
- [2] I.-H. Chiang et al., *AGS Experimental Proposal 926* (1996).
- [3] G.S. Atoian, *et. al.*, Nucl. Instr. and Meth. A **531**, 467 (2004).
- [4] R. Appel *et. al.*, Nucl. Instr. and Meth. A **479**, 349 (2002).
- [5] L. Aphecetche, *et al.* [ The PHENIX Collaboration ] Nucl. Instr. and Meth. A **499**, 521 (2003).
- [6] G. Avoni *et al.* [The HERA-B ECAL Collaboration], Nucl. Instr. and Meth. A **461**, 332 (2001).
- [7] F. Muheim [For the LHCb Collaboration], Nucl. Instr. and Meth. A **462**, 233 (2001).
- [8] GEANT, Detector description and simulation tool, CERN Program Library, Long Writeup W5013 (1994).
- [9] <http://www1.ihep.su/ihep/ihepsc/index.html> .
- [10] Kuraray Co., LTD, *Scintillation materials. Plastic fibers.*
- [11] S.P. Stoll, PHENIX Note #245 (1996).
- [12] I.G. Britvich *et al.* Instr. Exp. Tech. **44**, 472 (2001).

- [13] I.G. Britvich *et al.* Instr. Exp. Tech. **45**, 644 (2002).
- [14] J. Marler *et al.*, Nucl. Instr. and Meth. **449**, 311 (2000).
- [15] R.J. McIntyre, IEEE Trans. Electron Devices **ED-13**, 164 (1966).
- [16] D. H. Dowell *et al.*, Prog. Rep. BNL 37623 (1985), p. 29.
- [17] H. Huang and K. Kurita, AIP Conf. Proc. **868**, 3 (2006).
- [18] W.L. Reiter *et al.*, Nucl. Instr. and Meth. **173**, 275 (1980).
- [19] A. Fyodorov *et al.*, Nucl. Instr. and Meth. **A413**,352-356 (1998).